Structure of spontaneous periodic deformations in hybrid aligned nematic layers

Dariusz Krzyżański* and Grzegorz Derfel
Institute of Physics, Technical University of Łódź, ul. Wólczańska 219, 93-005 Łódź, Poland
(Received 17 July 2000; published 17 January 2001)

Periodic deformations, arising spontaneously in hybrid nematic layers were investigated numerically. So called splay stripes, which appear when the surface anchoring energy of the planar alignment was greater than that of the homeotropic alignment, were considered. Conical degeneration of the anchoring is assumed. The role of the layer thickness d and the anchoring strength W was studied by means of the dimensionless control parameter $\gamma = Wd/k_{11}$ defined for each boundary. The saddle-splay elastic constant k_{24} was varied within the limits given by general Ericksen inequalities. The director distributions were calculated. Two structures with different properties were distinguished: one for $k_{24}<0$ (mode 1) and the other for $k_{24}>0$ (mode 2). For given nematic liquid crystal parameters, mode 1 existed when γ exceeds some critical value. Below this critical γ, the director distortion decayed and the spatial period simultaneously diverged to infinity. As a result mode 1 disappeared and the homogeneously planar orientation was realized. The width of the stripes also increased infinitely for high γ. No upper limit of the γ range in which mode 1 could exist was found. Mode 2 existed for γ ranging from 0 to a certain critical value. Above this limit the periodic structure was replaced by the homogeneous hybrid alignment as a consequence of an infinite increase of the stripes' width. When $k_{24}>0$ was sufficiently small, the γ range was bounded from below, and a homogeneously planar orientation appeared for low γ. The visibility of the stripes between crossed polarizers was estimated by calculations of light transmission. In general, the stripes for $k_{24}<0$ turned out to be more distinct than that for $k_{24}>0$.

DOI: 10.1103/PhysRevE.63.021702 PACS number(s): 61.30.Cz, 61.30.Gd

I. INTRODUCTION

Hybrid anchoring conditions in the nematic layer usually induce two alternative structures. Typically, the director distribution is distorted with comparable contributions of splay and bend, resulting in a so called hybrid aligned nematic layer. However, if the layer is thinner than the threshold value d_c, the director field is uniform [1]. A uniform planar distribution occurs when planar anchoring prevails. In the opposite case (when the homeotropic anchoring dominates), the uniform distribution is homeotropic.

In 1990, another possibility was found experimentally by Lavrentovich and Pergamenshchik [2] in thin layers with a hybrid orientation. The nematic was deposited on the surface of glycerin with the upper surface free. The director alignment was planar at the liquid crystal-glycerin interface, and nearly homeotropic at the free surface. Azimuthal degeneration of the anchoring conditions was expected due to the isotropic character of the ambient media. The stripes, visible under a polarizing microscope, revealed the periodically deformed structure. (Similar periodic patterns were observed in layers with pure planar [3] and pure homeotropic [4] surface conditions, and in the twisted structures [5] under the influence of external fields. In the hybrid case, however, stripes can arise spontaneously, even without the action of any field.)

This effect was intensively studied theoretically [6–10]. Two types of periodic structures were predicted: splay stripes, when the planar anchoring is stronger than the homeotropic one, and bend stripes in the opposite case. This paper is devoted to splay stripes. Our aim was to investigate numerically the structure of the splay stripes and conditions for their occurrence. We focused on the case of 5CB—one of the substances used in experiments reported in Refs. [2], [11] and [12]. We calculated the director distribution within a single stripe and determined the ranges of layer parameters which allow the periodic states to exist. We also estimated the visibility of the stripes as observed in a microscope by calculating the light transmission through the system consisting of the nematic layer placed between crossed polarizers.

In Sec. II the details of the considered system are given, and the method of computation is described. Section III presents results, and Sec. IV is devoted to a short discussion of these.

II. METHOD

Our numerical calculations concerned the two-dimensional deformations possible in the infinite nematic layer of thickness d placed between two plates parallel to the (x,y) plane and positioned at $z=\pm d/2$. Two angles were necessary for a description of the director distribution: θ [measured between $\mathbf{n}$ and the (x,y) plane] and φ [between the x axis and the projection of $\mathbf{n}$ on the (x,y) plane]. We chose a coordinate system in which the stripes were directed along the x axis. The angles θ and φ depended on y and z. The y dependencies were periodic. The periodicity can be described by the wave vector $\mathbf{q}\|y$ or by the spatial period $\lambda = 2\pi/q$, where $q=|\mathbf{q}|$. The ratios of the elastic constants $k_b = k_{33}/k_{11}$ and $k_t = k_{22}/k_{11}$ close to that of 5CB were chosen to be $k_b = 1.3$ [13] and $k_t = 0.5$ [14].

In accordance with the anchoring conditions applied in the experiments [2,11,12], we assumed conically degenerated anchoring. This means that the anchoring energy does not depend on the azimuthal angle φ. The planar alignment

*Author to whom correspondence should be addressed.

was assumed at $z=-d/2$, and the homeotropic one at $z=d/2$. The finite anchoring energy was expressed in form

$$f_{\text{anchoring}}=-(\tfrac{1}{2})W_P\cos^2\theta_P-(\tfrac{1}{2})W_H\sin^2\theta_H, \qquad (1)$$

where W_P, W_H, θ_P, and θ_H are the anchoring strength parameters and director tilt angles corresponding to planar and homeotropic boundaries, respectively. In the following, the dimensionless quantities $\gamma_P=W_Pd/k_{11}$ and $\gamma_H=W_Hd/k_{11}$ are used. They measure the influence of the boundary conditions on the layer structure. Low values of these parameters correspond to thin layers, weak anchoring, and/or high elastic constant. They are due to the high effective curvature stiffness of the layer. The director field in such a layer is then resistive to deformations. On the other hand, high values of γ correspond to effectively soft layers in which the director field is susceptible to distortions. The calculations were performed for layers which were characterized by various γ_P and γ_H for three ratios $p=\gamma_P/\gamma_H$: $p=10$, $p=2$ (which we recognize as high and medium, respectively), and $p=1.137$ (which was estimated in the experiment reported in Ref. [11]).

In the case of structures which are deformed at the boundaries (due to the finite anchoring strength) and spatially modulated along them (here along y), the elastic free energy density contains a term depending on the saddle-splay elastic constant k_{24}. The ratios of the elastic constants k_{22}/k_{11} and k_{24}/k_{11} are related by the inequalities which stem from general rules:[15]

$$k_{24}/k_{11}\leqslant 2-k_{22}/k_{11},$$
$$-k_{22}/k_{11}\leqslant k_{24}/k_{11}\leqslant k_{22}/k_{11}. \qquad (2)$$

In our computations, the values of $k_s=k_{24}/k_{11}$ ratios were changed throughout the entire allowed range $(-0.5,0.5)$. The other surfacelike elastic constant k_{13} was assumed to be zero, according to the theoretical result obtained by Yokoyama [16].

A single stripe of width λ was considered during the computations. Periodic boundary conditions along the y axis were imposed. The structure of the stripe was found by numerical minimization of the free energy per unit area of the layer. This quantity was expressed as the energy of the stripe, counted per unit length along the x axis, divided by the width λ. The corresponding formula takes a form (with accuracy to an unimportant constant)

$$F=\frac{k_{11}}{2\lambda}\int_0^{\lambda}\Bigg\{\int_{-d/2}^{d/2}\{(\nabla\mathbf{n})^2+k_t[\mathbf{n}\cdot(\nabla\times\mathbf{n})]^2 +k_b[\mathbf{n}\times(\nabla\times\mathbf{n})]^2\}dz+2(k_t+k_s)[\mathbf{n}_P\cdot(\nabla\mathbf{n}_P) +\mathbf{n}_P\times(\nabla\times\mathbf{n}_P)-\mathbf{n}_H\cdot(\nabla\mathbf{n}_H)-\mathbf{n}_H\times(\nabla\times\mathbf{n}_H)] +\frac{W_P}{k_{11}}(\mathbf{n}_P\cdot\mathbf{z})^2-\frac{W_H}{k_{11}}(\mathbf{n}_H\cdot\mathbf{z})^2\Bigg\}dy, \qquad (3)$$

where $\mathbf{z}$ is versor directed along the z axis. By introducing the reduced quantities $\eta=y/\lambda$ and $\zeta=z/d$, the dimensionless form of the integrands in Eq. (3) can be obtained, where $\nabla=((d/\lambda)(\partial/\partial\eta),\partial/\partial\zeta)$:

$$F=\frac{k_{11}}{2d}\int_0^1\Bigg\{\int_{-1/2}^{1/2}\{(\nabla\mathbf{n})^2+k_t[\mathbf{n}\cdot(\nabla\times\mathbf{n})]^2 +k_b[\mathbf{n}\times(\nabla\times\mathbf{n})]^2\}d\zeta+2(k_t+k_s)[\mathbf{n}_P\cdot(\nabla\mathbf{n}_P) +\mathbf{n}_P\times(\nabla\times\mathbf{n}_P)-\mathbf{n}_H\cdot(\nabla\mathbf{n}_H)-\mathbf{n}_H\times(\nabla\times\mathbf{n}_H)] +\gamma_P(\mathbf{n}_P\cdot\mathbf{z})^2-\gamma_H(\mathbf{n}_H\cdot\mathbf{z})^2\Bigg\}d\eta, \qquad (4)$$

In this way the free energy density per unit area of the layer F can be expressed in units equal to k_{11}/d.

The director distribution over the cross section of the stripe, described by the functions $\theta(\eta,\zeta)$ and $\varphi(\eta,\zeta)$, was approximated by discrete angles θ_{ij} and φ_{ij} defined in the sites of the $M\times N$ regular lattice. The indices $i=1,\ldots,M$ and $j=1,\ldots,N$ determined the positions along the y and z axes, respectively. The coordinates $\eta=0$ and 1 were determined by $i=1$ and $i=M+1$. The lattice sites at the boundary plates with $\zeta=-\frac{1}{2}$ and $\frac{1}{2}$ were labeled by $j=1$ and $j=N$. In most cases $M=48$ and $N=17$; in the case of strong distortions, however, M was increased up to 64. The planes determined by $i=$const and $j=$const [parallel to the (x,y) and (x,z) planes respectively], divided the cross section of the stripe into $M\times(N-1)$ rectangular cells. The average angles θ and φ for each cell, as well as their spatial derivatives were expressed by means of θ_{ij} and φ_{ij}. These values were used to calculate the elastic free energy of the cell counted per unit length in the x direction. The energy of the cells adjacent to the boundary plates were supplemented by the surface anchoring terms expressed by use of θ_{i1}, θ_{iN}, φ_{i1}, and φ_{iN}. A sum of the energies related to all the $M\times(N-1)$ cells divided by λ was equal to the total free energy per unit area of the layer.

Initially, the values $\theta_{ij}=0$ and $\varphi_{ij}=0$ for all i and j, and the ratio $\lambda/d=1$, were imposed. To start the deformation, a small deviation from the initial director position at one arbitrarily chosen site of the lattice was introduced. The final set of the θ_{ij} and φ_{ij} and λ/d variables, which approximated the real equilibrium director distribution, was calculated using an iteration process. During the computations, these variables were varied successively by small intervals. The free energy per unit area of the layer was calculated after each change. New values of the variables were accepted if they led to a lower free energy. This procedure was repeated until no further reduction in the total free energy could be achieved. Then the interval was decreased and the process repeated. As a result, a state with minimum energy was obtained. A similar procedure was applied successfully to investigations of periodic deformations in other systems [17].

The resulting discrete director distributions possessed interesting symmetry properties along the y direction:

$$\theta(\eta,\zeta)=\theta(0.5-\eta,\zeta)=-\theta(0.5+\eta,\zeta)=-\theta(1-\eta,\zeta), \qquad (5)$$

$$\varphi(\eta,\zeta) = -\varphi(0.5-\eta,\zeta) = -\varphi(0.5+\eta,\zeta) = \varphi(1-\eta,\zeta).$$

We used this symmetry by computing the director distribution only in one quarter of the stripe cross section, i.e., for $i=1,\ldots,M/4$. The results were suitably copied for the rest of the stripe. We approximated the $\theta(\zeta)$ and $\varphi(\zeta)$ functions by the polynomials

$$\theta(\eta,\zeta) = \sum_{k=0}^{K} a_k(\eta)\zeta^k \tag{6}$$

and

$$\varphi(\eta,\zeta) = \sum_{k=0}^{K} b_k(\eta)\zeta^k, \tag{7}$$

and found that $K=3$ was sufficient in all cases. Therefore, energy minimization was possible by changing the a_k and b_k coefficients instead of θ_{ij} and φ_{ij}. The set of angles obtained in this way for some choice of parameters of the system served as a starting point for computations of another parameters.

The limiting values of the system parameters separating the planar structure from the periodically deformed structure can be analyzed using a small angle approximation. The free energy per unit area of the weakly deformed layer reduces to

$$F = \frac{k_{11}}{2d}\int_0^1 \Bigg\{ \int_{-1/2}^{1/2} [\varphi_\eta^2 + \theta_\zeta^2 + 2\varphi_\eta\theta_\zeta + k_t(\theta_\eta^2 + \varphi_\zeta^2 - 2\theta_\eta\varphi_\zeta)]d\zeta + 2(k_t+k_s)[-\varphi_P\theta_{\eta P} + \theta_P\varphi_{\eta P} + \varphi_H\theta_{\eta H} - \theta_H\varphi_{\eta H}] + \gamma_P\theta_P^2 - \gamma_H\theta_H^2 \Bigg\} d\eta \tag{8}$$

where P and H refer to the planar and homeotropic boundary and the differentiation with respect to η, and ζ is denoted by the corresponding indices.

The set of the linearized Euler-Lagrange equations takes the forms

$$k_t\theta_{\eta\eta} + (1-k_t)\varphi_{\eta\zeta} + \theta_{\zeta\zeta} = 0,$$

$$\varphi_{\eta\eta} + (1-k_t)\theta_{\eta\zeta} + k_t\varphi_{\zeta\zeta} = 0. \tag{9}$$

Its solutions depend on four constants C_1, C_2, C_3, and C_4:

$$\theta(\eta,\zeta) = \{[C_1((s/Q)-\zeta)-C_2]\exp(Q\zeta) + [C_3((s/Q)+\zeta)+C_4]\exp(-Q\zeta)\}\cos Q\eta,$$

$$\varphi(\eta,\zeta) = [(C_1\zeta+C_2)\exp(Q\zeta) + (C_3\zeta+C_4)\times\exp(-Q\zeta)]\sin Q\eta, \tag{10}$$

where $s=(1+k_t)/(1-k_t)$, and $Q=qd$ is the dimensionless wave number. The constants are determined by the boundary conditions

$$\theta_{\zeta P} + (1-2k_t-2k_s)\varphi_{\eta P} - \gamma_P\theta_P = 0,$$

$$k_t\varphi_{\zeta P} + (k_t+2k_s)\theta_{\eta P} = 0,$$

$$\theta_{\zeta H} + (1-2k_t-2k_s)\varphi_{\eta H} - \gamma_H\theta_H = 0,$$

$$k_t\varphi_{\zeta H} + (k_t+2k_s)\theta_{\eta H} = 0. \tag{11}$$

When functions (10) are substituted into Eqs. (11), a system of linear equations arises, which possesses a nontrivial solution if and only if its determinant vanishes:

$$\begin{vmatrix} (A-\gamma_P B)P^* & (G+\gamma_P)P^* & (-C+\gamma_P D)P & (G-\gamma_P)P \\ (E-C)P^* & GP^* & (E-A)P & -GP \\ (C+\gamma_H D)P & (G+\gamma_H)P & (-A-\gamma_H B)P^* & (G-\gamma_H)P^* \\ (E-A)P & GP & (E-C)P^* & -GP^* \end{vmatrix} = 0, \tag{12}$$

In Eq. (12) the abbreviations $A=(k_t+k_s)Q+2k_t/(1-k_t)$, $B=1/2+(1+k_t)/[Q(1-k_t)]$, $C=-(k_t+k_s)Q+2k_t/(1-k_t)$, $D=1/2-(1+k_t)/[Q(1-k_t)]$, $E=2(k_t+k_s)(1+k_t)/(1-k_t)$, $G=-2(k_t+k_s)Q$, $P=\exp(Q/2)$, and $P^*=\exp(-Q/2)$ were used.

Equation (12) gives the relation between Q and the parameters of the layer. In particular, the $\gamma_P(Q)$ dependence can be found if the parameters k_b, k_t, k_s, and p are constant. Extremes of this function, γ_{P1}, determine the condition for arising of periodic deformations of the wave vector Q_1. The γ_{P1} values, calculated for various values of k_s, determine the lower boundary of the region of existence of the stripes in the (γ_P, k_s) plane.

The light transmission through the system consisting of the periodically deformed layer placed between crossed polarizers was calculated by the Mueller matrix method [18] applied to a single stripe. The stripe was divided into M segments and $N-1=1024$ sublayers. The directions of the optical axes in these sublayers were determined by means of $N=1025$ pairs of angles of θ_{ij} and φ_{ij}, which were calculated by use of polynomials (6) and (7). A thickness $d=1\ \mu$m was assumed. The light transmission was calculated by use of 5CB room temperature refractive indices: $n_o=1.532$ and $n_e=1.726$ [19] for the yellow light wavelength

$\Lambda = 589$ nm. Due to the small thickness, the assumption of normal incidence of the light beam on each sublayer was justified. The light transmission was obtained as

$$T = I_N / I_0, \tag{13}$$

where I_0 and I_N are the intensities of the incident and emerging light, respectively, given by the first components of the corresponding Stokes vectors $\mathbf{S}_0$ and $\mathbf{S}_N$. The light incident on the liquid crystal layer was assumed to be linearly polarized (with polarization direction making an angle $\pi/4$ with $\mathbf{q}$) and determined by the Stokes vector $\mathbf{S}_0$. The subsequent Stokes vectors of the light emerging from the lth sublayer, for $l = 1, \ldots, N-1$, are given by

$$\mathbf{S}_l = \mathbf{M}_l \mathbf{S}_{l-1}, \tag{14}$$

where $\mathbf{M}_l$ is the Mueller matrix of the lth sublayer. The Stokes vector of the emerging light is

$$\mathbf{S}_N = \mathbf{A}\mathbf{S}_{N-1}, \tag{15}$$

where $\mathbf{A}$ is the Mueller matrix of the analyzer.

As a measure of visibility we defined the ratio [20]

$$V = (T_{\max} - T_{\min})/(T_{\max} + T_{\min}), \tag{16}$$

where $T_{\max}$ and $T_{\min}$ are the maximum and minimum transmissions, respectively. We assumed that stripes were observable when $V > 0.1$.

III. RESULTS

Two types of the director distributions in periodically deformed hybrid layer were found: one type for negative k_s values and another type for positive values of the k_s ratio. Their properties will be presented separately in the following.

A. $k_s < 0$ (mode 1)

A typical director distribution within a well developed stripe obtained for $k_s < 0$ is illustrated in Fig. 1 by means of cylinders which symbolize the directors. Two halves of the stripe with opposite senses of director distribution can be distinguished. The director is confined to the surface of a cone with an oval base and an axis parallel to x. By moving along y over the distance λ at constant z, one observes that the director rotates continuously around the cone axis by an angle 2π. The shape of the cone depends on z. This structure is determined quantitatively by plots of the functions $\theta(\eta, \zeta)$ and $\varphi(\eta, \zeta)$ shown in Fig. 2. For given η, the angle θ changes almost linearly with ζ, whereas φ is nearly constant.

The spatial period of the deformation, λ, depends on the parameters γ_P and γ_H. Since the calculations were performed for constant ratios γ_P / γ_H, the results will be presented as functions of γ_P. Figures 3(a)–3(c) show the behavior of the spatial period by means of plots of Q as functions of γ_P for several values of k_s and for the three p ratios. The minimum spatial period exceeds several times the thickness of the layer. A well defined critical value γ_{P1}, which limits the range of existence of the stripes from below, is evident. Close to the limit γ_{P1}, when the layer is ''stiff,'' the periodic deformation is weak and the η dependence of the angles is sinusoidal with small amplitudes $\theta_m(\zeta)$ and $\varphi_m(\zeta)$. When γ_P tends to γ_{P1}, the amplitudes $\theta_m(\zeta)$ and $\varphi_m(\zeta)$ decrease to zero. Linear analysis, justified in this circumstance, gives $Q_1 = 0$. In this way the homogeneous pla-

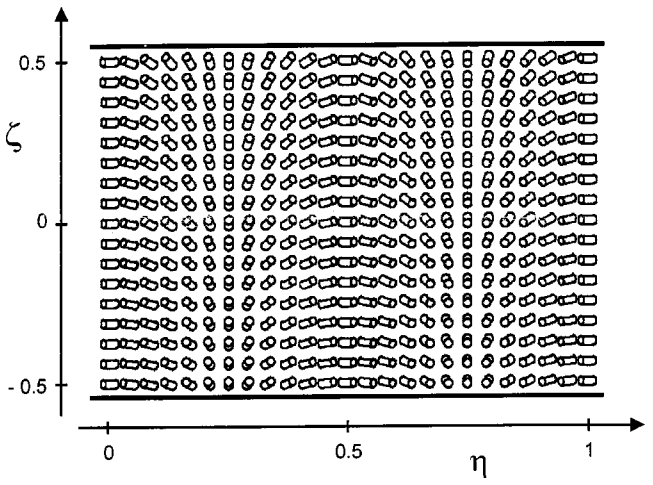

FIG. 1. Typical director distribution for the single stripe of mode 1: $p = 2$, $k_s = -0.3$, $\gamma_P = 1.4$, and $\lambda/d = 34$.

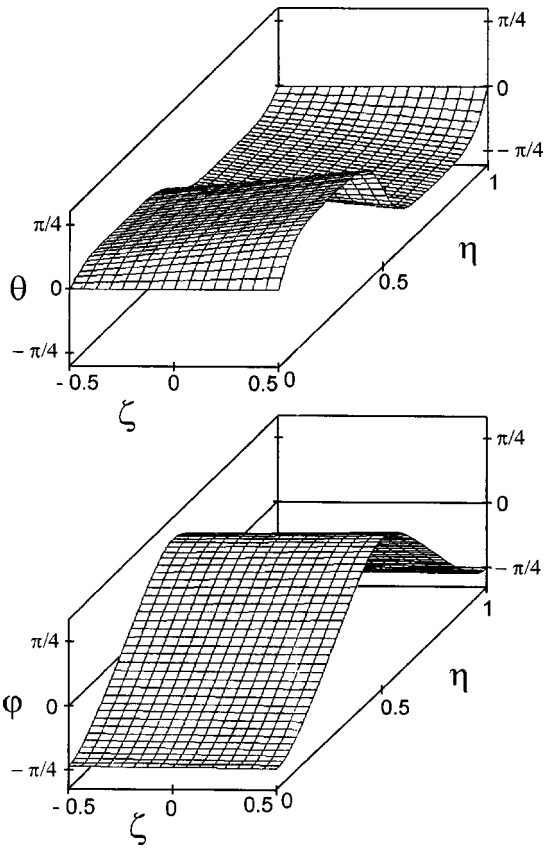

FIG. 2. The angles θ and φ for the typical single stripe of mode 1: $p = 2$, $k_s = -0.3$, $\gamma_P = 1.4$, and $\lambda/d = 34$.

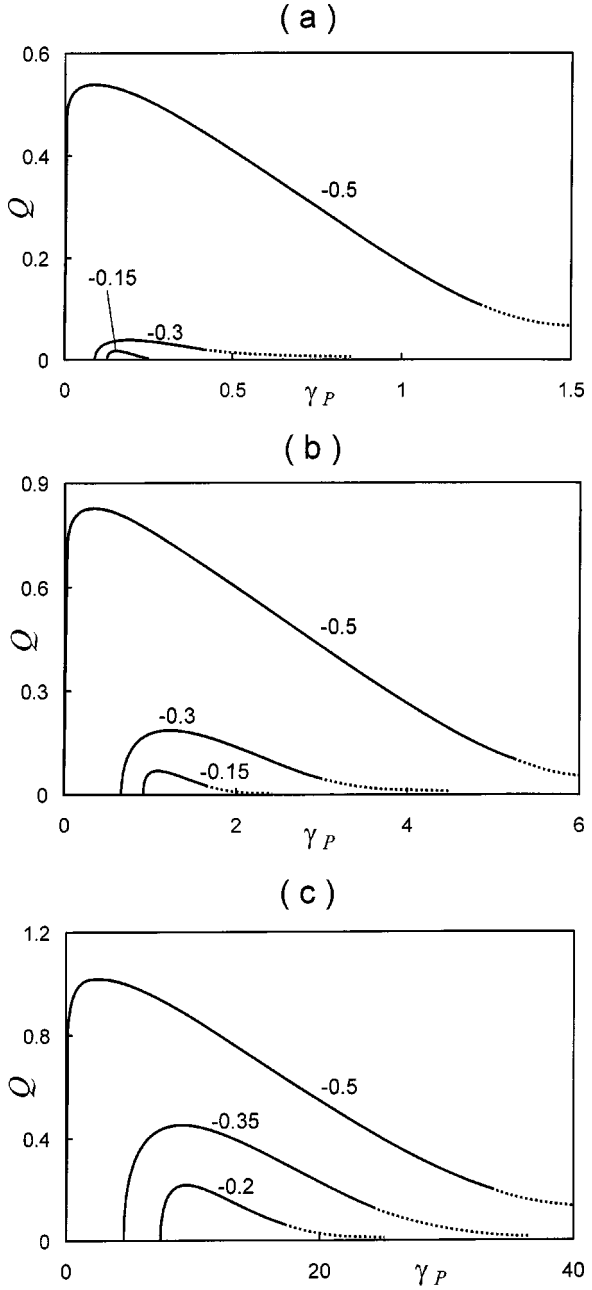

FIG. 3. The dimensionless wave number Q of mode 1 as a function of the planar anchoring parameter γ_P for the k_s values indicated at each curve: (a) $p=1.137$, (b) $p=2$, and (c) $p=10$. The dotted lines correspond to the periodic deformations for which the free energy is higher than the energy of the homogeneous hybrid structure.

nar structure arises when $\gamma_P<\gamma_{P1}$. For high γ_P, when the layer is ''soft,'' the deformation is strong. The period of the strongly deformed structure also increases with γ_P, but does not diverge for any finite γ_P.

The dependence of γ_{P1} on k_s is shown in Fig. 4. It can be found using linear analysis, and expressed in a normalized form, common for any $p=\gamma_P/\gamma_H$ ratio,

$$\gamma_{P1}/\gamma_c=4(k_t+k_s)(1-k_t-k_s), \tag{17}$$

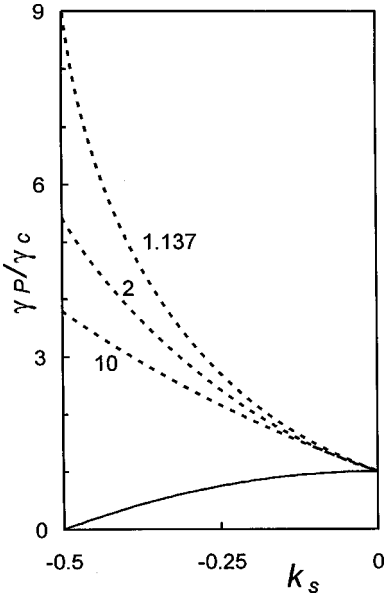

FIG. 4. The regions of existence of the periodically deformed state. The solid line, common for all p, presents the normalized critical anchoring strength parameter γ_{P1}/γ_c as a function of the negative saddle-splay elastic constant k_s. The dashed lines show γ_P/γ_c values corresponding to the equality of the free energies of the periodic and homogeneous hybrid states (see Sec. IV). The p ratios are indicated.

where $\gamma_c=p-1$ is the critical value separating the homogeneous hybrid and homogeneous planar orientations. When k_s tends to -0.5, i.e., to $-k_t$, the lower critical limit γ_{P1} tends to 0. The results of the numerical minimization of the free energy agreed very well with Eq. (17).

The dependence of λ on the k_s ratio is illustrated in Fig. 5 by the function $Q(k_s)$ plotted for $\gamma_P=\gamma_c$. The spatial period tends asymptotically to infinity when k_s tends to 0. In the vicinity of $k_s=0$, the power law $Q=|k_s|^\alpha$ is approximately satisfied with $\alpha\approx 1.2$ for each p.

B. $k_s>0$ (mode 2)

For a positive k_s ratio, the director distribution is different from that of mode 1 (Fig. 6). As previously, the director

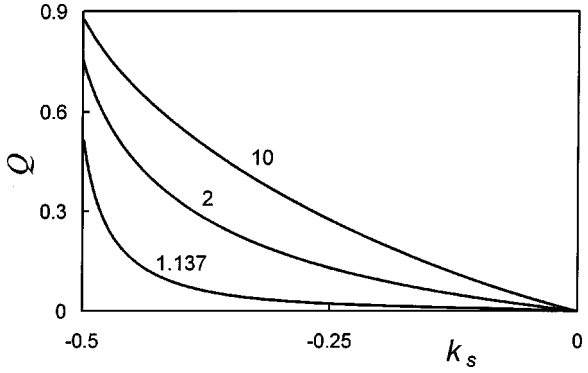

FIG. 5. The dimensionless wave number Q as a function of the negative saddle-splay elastic constant k_s for $\gamma_P=\gamma_c$; the p values are indicated for each curve.

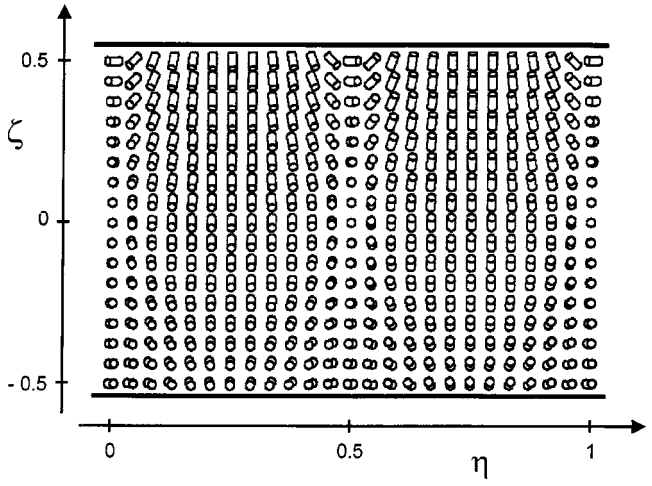

FIG. 6. The typical director distribution for the single stripe of mode 2: $p=2$, $k_s=0.25$, $\gamma_P=5$, and $\lambda/d=4.6$.

rotates around the x axis on the surface of a cone. However, the senses of the rotation in various parts of the layer are different. Close to the planar wall the structure is very similar to that of the $k_s<0$ case. In the neighborhood of the homeotropic wall, the rotation is reversed. The plots of the functions $\theta(\eta,\zeta)$ and $\varphi(\eta,\zeta)$ are presented in Fig. 7.

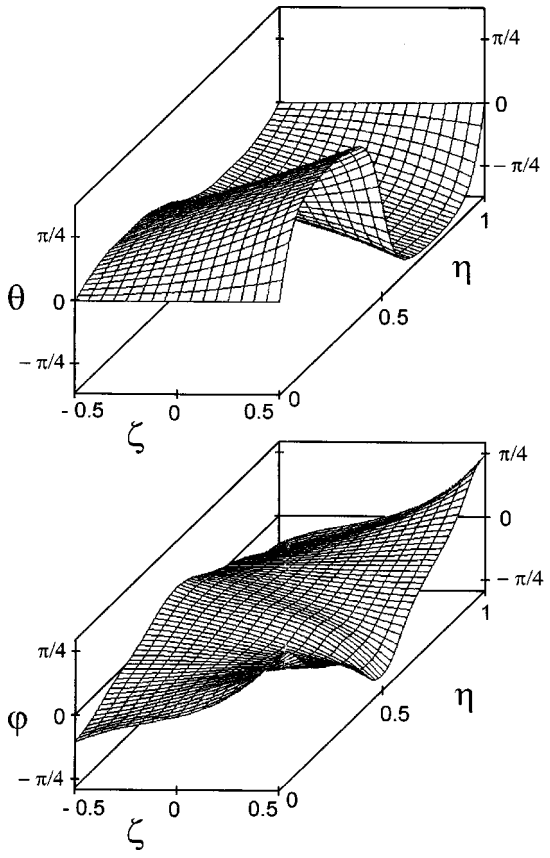

FIG. 7. The angles θ and φ for the typical single stripe of mode 2: $p=2$, $k_s=0.25$, $\gamma_P=5$, and $\lambda/d=4.6$.

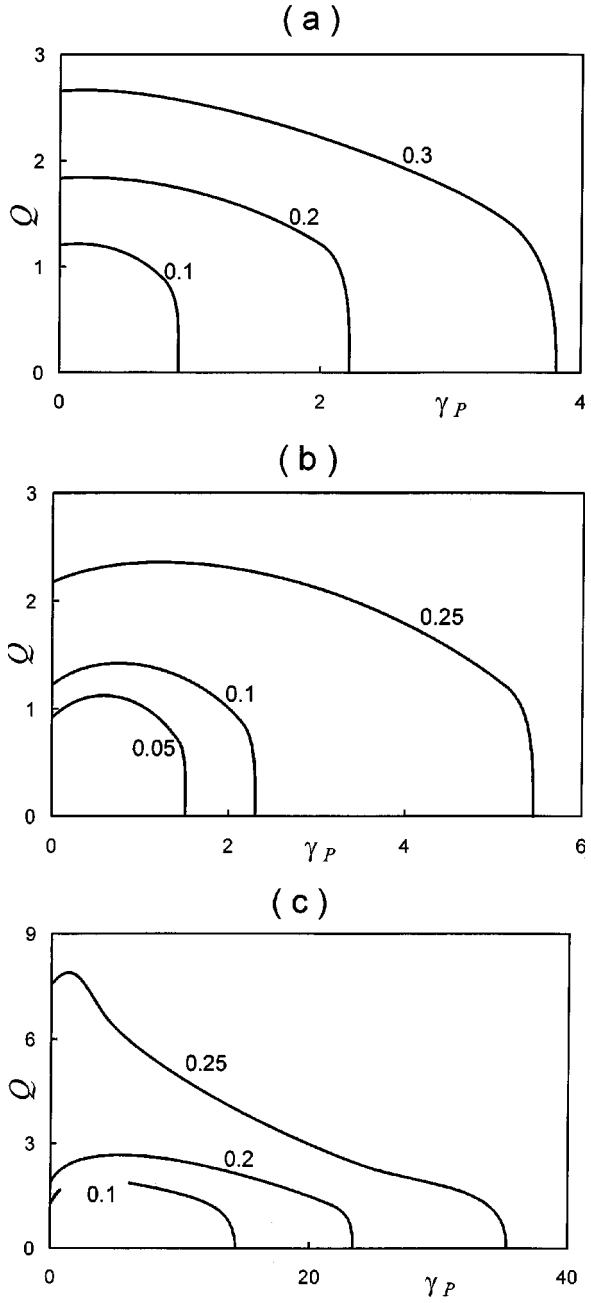

FIG. 8. The dimensionless wave number Q of mode 2 as a function of the planar anchoring parameter γ_P for the k_s values indicated at each curve: (a) $p=1.137$, (b) $p=2$, and (c) $p=10$. In (c) the two branches of the $k_s=0.1$ curve correspond to two ranges of the stripes' existence.

For high values of γ_P, the deformation is strong. Both angles θ and φ depend significantly on z. The width of the stripes depends on γ_P, as illustrated in Figs. 8(a)–8(c) by plots of Q as functions of γ_P for several values of k_s, and for the three p values. The narrowest width of the stripes is smaller than the layer thickness. Nevertheless the stripes become wider with increasing γ_P. When γ_P approaches the upper limiting value γ_{P2}, λ tends rapidly to infinity. The angles θ in the two halves of the stripe become nearly inde-

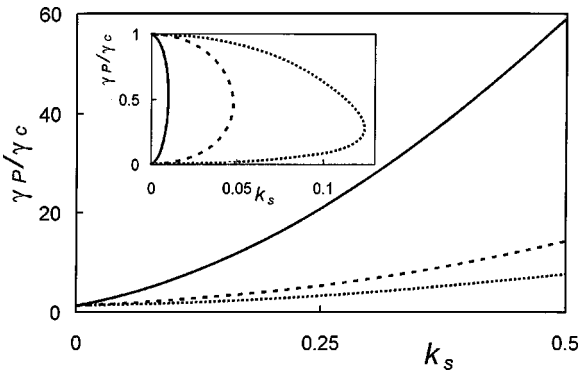

FIG. 9. Regions of existence of the periodically deformed state for the positive saddle-splay elastic constant k_s. The inset shows the details for $\gamma_P/\gamma_c \leqslant 1$; solid line: $p=1.137$; dashed line: $p=2$; dotted line: $p=10$. In the main figure, the periodically deformed state takes place below each curve, whereas the homogeneous hybrid alignment is realized above it. In the inset, the periodic state occurs on the right-hand side of each curve, and the uniform planar orientation appears on the left side.

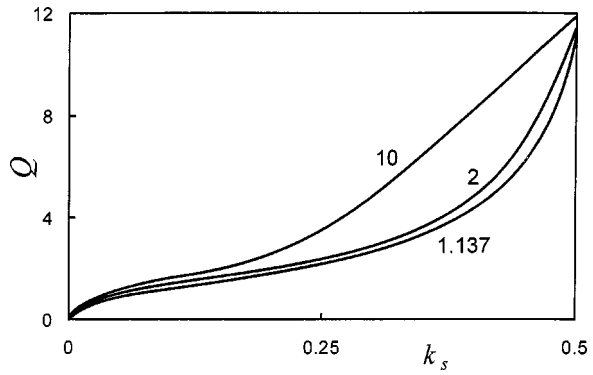

FIG. 10. The dimensionless wave number Q as a function of the positive saddle-splay elastic constant k_s for $\gamma_P=\gamma_c$; the p values are indicated for each curve.

pendent of y over a significant part of each half, and take values corresponding to the homogeneous hybrid structure. The angles φ become close to zero, with the exception of narrow regions (''walls'') between the halves. The nearly homogeneous regions in each half of a stripe spread over the whole layer and the homogeneous hybrid structure replaces the periodic state.

In a narrow range of $k_s>0$ in vicinity of $k_s=0$, there are two ranges of γ_P for which periodic deformations can be realized: $0<\gamma_P<\gamma'_{P1}$ and $\gamma''_{P1}<\gamma_P<\gamma_{P2}$. They are separated by a gap in which the planar state takes place. The limiting values γ'_{P1} and γ''_{P1}, calculated by numerical minimization of the free energy, and those derived from the linear analysis coincide. The amplitudes $\theta_m(\zeta)$ and $\varphi_m(\zeta)$ decrease to zero when $\gamma_P \to \gamma'_{P1}$ or $\gamma_P \to \gamma''_{P1}$, whereas the wavelengths λ remain finite. For higher k_s, the gap between γ'_{P1} and γ''_{P1} disappears. This means that in the prevailing part of the positive k_s range the homogeneous planar state is forbidden. The stripes of finite width may exist down to $\gamma_P=0$. The amplitudes $\theta_m(\zeta)$ and $\varphi_m(\zeta)$ reach a minimum for some γ_P and do not vanish. Figure 9 summarizes the above statements, showing the regions of existence of the interesting states in the $(\gamma_P/\gamma_c, k_s)$ plane for the three p ratios. The uniform planar alignment can exist only in the narrow range of k_s in vicinity of $k_s=0$. This range increases with p. The upper limit γ_{P2} grows with k_s.

Figure 10 shows the dependence of the spatial period on k_s for $\gamma_P=\gamma_c$. The spatial period diverges to infinity when k_s tends to 0 according to approximate power law $Q=k_s^{\beta}$, where $\beta \approx 0.5$ for each p.

C. Visibility of the stripes

The calculations of light transmitted through the different parts of a stripe when the layer is placed between crossed polarizers (making angles of $\pm\pi/4$ with the stripes) allow one to an estimate of their visibility. Figure 11 shows three examples of the $T(\eta)$ functions for a high contrast stripe, for a poorly visible stripe and for a stripe with an additional dark line in the middle of the central bright band. (Such a pattern corresponds to the experimental observations [11].) It was found that the stripes of mode 1 were distinct almost in the whole range of their existence, whereas only the strong periodic deformations of mode 2 were visible when they appeared for sufficiently high $k_{24}>0$.

IV. DISCUSSION

Periodic deformations in the hybrid nematic layers are fairly complex phenomena. Their features depend on many parameters—three elastic constant ratios k_b, k_t, and k_s and at least two anchoring parameters γ_P and γ_H. In this paper, we found the structure of the splay stripes and determined the conditions for their existence. We focused on a single typical liquid crystal and chose the material param-

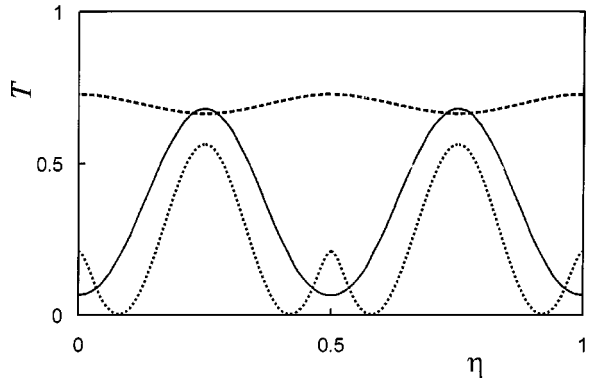

FIG. 11. The exemplary transmission of a single stripe between crossed polarizers $p=2$; solid line: a distinct stripe, $k_s=-0.15$, $\gamma_P=1.1$, and $\lambda/d=86$; dashed line: a poorly visible stripe, $k_s=0.05$, $\gamma_P=1$, and $\lambda/d=6.1$; dotted line: a ''doubled'' stripe, $k_s=-0.15$, $\gamma_P=1.6$, and $\lambda/d=166$.

eters of 5CB. We assumed a conical degeneracy of the surface anchoring. Since the value of the surfacelike elastic constant k_{24} is unknown, it was varied within the limits determined by the Ericksen inequalities. The crucial role of k_{24} described in Ref. [8] was confirmed. The properties of the small periodic deformations were studied using a linear analysis method.

Our results are consistent with the theoretical predictions made in Ref. [8]. The results described in Sec. III and some additional calculations mentioned below allow the main properties of the periodic deformations in the hybrid aligned nematic layers to be summarized as follows.

(i) There are two modes of the splay stripes, corresponding to two signs of the quantity $R=1-2k_t-2k_s$. They differ not only in the form of the director distribution but also in their minimum widths. For mode 1, λ is always greater than d, whereas for mode 2 the relation $\lambda<d$ can take place.

In our case, when $k_t=0.5$, R changes its sign at $k_s=0$. This explains the peculiar role of $k_s=0$. In Ref. [8], where $k_t=1$, there were also two ranges of k_s, separated by the gap centered at $k_s=-0.5$ (i.e., at $R=0$). We checked numerically that there were two different periodic modes in each of this ranges. Their structure was different from modes 1 and 2 illustrated in Figs. 1 and 6. This result reveals that one can expect many variants of the periodic director distributions corresponding to various material parameters and anchoring conditions. In particular the role of k_t seems to be equally important as that of k_s.

(ii) The stripes of mode 1 were found for arbitrarily high γ_P. We relate this result to the conical degeneracy of the surface anchoring. We checked numerically that when the rotations of the surface director around the z axis were hindered (as assumed in Ref. [8]), the wave number of the periodic structure decreased to zero for finite γ_P. This denotes the existence of an upper boundary γ_{P2} between the stripes and the homogeneous hybrid regions due to the infinite divergence of the spatial period.

In the case of the conical degeneracy, one can tentatively estimate the extent of the periodic state by comparing its free energy per unit area with the energy of the homogeneously hybrid aligned layer. With this approach, the upper limits γ_{P2} correspond to the equality of these energies. They are shown in Fig. 4 by dashed lines. In real samples, the lateral boundaries and other imperfections can limit the largest possible width of the stripe.

Another effect, which we relate to the conical degeneracy, is the divergence of the mode 1 spatial period when γ_P tends to γ_{P1}. The results of Ref. [8], and our additional calculations, showed finite λ at γ_{P1} if nondegenerated anchoring conditions were imposed. On the other hand, when the conical degeneracy is introduced to equations used in Ref. [8], the divergence is obtained.

(iii) For sufficiently high positive k_s, the γ_P range of the stripes occurrence spreads down to $\gamma_P=0$. (This effect was also presented in Ref. [8] for $k_s>0$.) For small values of positive k_s, we found two ranges of γ_P (Fig. 10) separated by a gap for which the uniform planar orientation was realized.

The experimental data presented in Ref. [11] show that the spatial period λ depends monotonically on the layer thickness d, and range of d in which the stripes were observed was bounded from above. Qualitatively, behavior of this type corresponds to mode 2 if not very small γ_P values are considered. However, the stripes of mode 2 are rather narrow, and λ is comparable with d in a wide range of γ_P. The narrowest observed stripes were about ten times wider than d, so they cannot be identified with mode 2. As concerns mode 1, the experimental evidence of the uniform planar orientation for very thin layers [2] corresponds to its properties. The experimental dependence $\lambda(d)$ is also comparable with numerical data found for mode 1 (when γ_P is not extremely small). However, the experiment shows some signs of divergence of the $\lambda(d)$ function, suggesting the existence of an upper limiting value γ_{P2}, which was not found numerically. Summarizing, a qualitative agreement between the experimental data and the numerical results cannot be fully achieved either for mode 1 or mode 2 if conical degeneracy is assumed.

As stated above in (ii), the limit γ_{P2} appears, and $\lambda(\gamma_{P1})$ becomes finite when the surface director rotations about the z axis are hindered. It seems to be plausible that numerical simulations of mode 1 would give results consistent with the experimental data, if the surface anchoring conditions were nondegenerated. Therefore, we suggest that assumptions concerning the degeneracy of the surface anchoring or the ideal planar and homeotropic conditions do not exactly reflect the real physical situation taking place during the experiments. We hope that future experiments will yield additional material for verification of corresponding numerical simulations.

The periodic deformations described in this paper can be considered as an interesting example of the pattern formation phenomena which are observed in various physical systems [21]. In general, spatially periodic patterns arise under the influence of external excitation when some threshold value of a suitable stress parameter is exceeded. The system becomes unstable to infinitesimal perturbations with wave vector $\mathbf{q}_0$ which are amplified. A new equilibrium state arises with the appearance of self-organization and order, which is seen as a pattern.

For potential systems such as hybrid aligned nematic layers, the amplitude of the perturbations is governed by equations which have the form of equilibrium conditions for forces or torques. In our case, the corresponding equations concern the elastic, viscous, and surface torques exerted on the director. The γ_P/γ_c ratio can be adopted as a proper measure of the excitation. The small angles θ and φ can be treated as perturbations of the uniform planar state. Their time evolution can be described by exponential term $\exp(\sigma t)$, where σ is the growth rate. A detailed analysis of the growth of the instability is beyond the scope of this paper. Nevertheless let us note that the result of linear analysis expressed by Eq. (17) corresponds to the critical value $\sigma=0$, which separates the conditions for damping the perturbations ($\sigma<0$) from the conditions for amplifying them ($\sigma>0$).

[1] G. Barbero and R. Barberi, J. Phys. (France) **44**, 609 (1983).
[2] O. D. Lavrentovich and V. M. Pergamenshchik, Mol. Cryst. Liq. Cryst. **179**, 125 (1990).
[3] F. Lonberg and R. B. Meyer, Phys. Rev. Lett. **55**, 718 (1985).
[4] P. Cladis and S. Torza, J. Appl. Phys. **46**, 584 (1975).
[5] V. I. Tsoy, G. V. Simonenko, and V. G. Chigrinov, Liq. Cryst. **13**, 227 (1993).
[6] A. Sparavigna, L. Komitov, B. Stebler, and A. Strigazzi, Mol. Cryst. Liq. Cryst. **207**, 265 (1991).
[7] A. Sparavigna, L. Komitov, and A. Strigazzi, Mol. Cryst. Liq. Cryst. **212**, 289 (1992).
[8] A. Sparavigna and A. Strigazzi, Mol. Cryst. Liq. Cryst. **221**, 209 (1992).
[9] A. Sparavigna, L. Komitov, P. Palffy-Muhoray, and A. Strigazzi, Liq. Cryst. **14**, 1945 (1993).
[10] V. M. Pergamenshchik, Phys. Rev. E **47**, 1881 (1993).
[11] O. D. Lavrentovich and V. M. Pergamenshchik, Phys. Rev. Lett. **73**, 979 (1994).
[12] O. D. Lavrentovich and V. M. Pergamenshchik, Int. J. Mod. Phys. B **9**, 251 (1995).
[13] M. J. Bradshaw, E. P. Raynes, J. D. Bunning, and T. E. Faber, J. Phys. (France) **46**, 1513 (1985).
[14] S. Faetti, G. Gatti, and V. Palleschi, J. Phys. (France) Lett. **46**, L-881 (1985).
[15] J. L. Ericksen, Phys. Fluids **9**, 1205 (1966).
[16] H. Yokoyama, Phys. Rev. E **55**, 2938 (1997).
[17] D. Krzyżański and G. Derfel, Phys. Rev. E **61**, 6663 (2000).
[18] A. Yariv and P. Yeh, *Optical Waves in Crystals* (Wiley, New York, 1984).
[19] P. P. Karat and N. V. Madhusudana, Mol. Cryst. Liq. Cryst. **36**, 51 (1976).
[20] M. Born and E. Wolf, *Principles of Optics* (Cambridge University Press, Cambridge, 1999).
[21] M. C. Cross and P. C. Hohenberg, Rev. Mod. Phys. **65**, 851 (1993).